Invited Paper

Matter-wave/atom interferometry

J. F. Clauser, and S. Li

Physics Department
University of California-Berkeley, Berkeley, CA 94720, USA.

ABSTRACT

Although interferometry's earliest and most familiar use is with photons, the discovery of matter-wave (deBroglie-wave) interference for electrons demanded the development of quantum mechanics. Since then, matter-wave interferometry has been performed with neutrons, Cooper electron-pairs, and most recently, with whole atoms and diatomic molecules. This talk describes our recent high-flux atom interferometry experiments using the generalized Talbot-vonLau effect. Our interferometer consists of a sequence of three planar vacuum-slit diffraction gratings, microfabricated from silicon nitride membranes. DeBroglie-wave interference fringes are sensed by measuring the transmission of potassium atoms on a hot-wire as a function of grating relative position. Different spatial Fourier components (up to sixth) in the diffraction pattern are resonant in the interferometer at different atomic velocities (i.e. at different wavelengths). When a laser cooled slow atomic beam is incident, various different diffraction patterns are observed as a function of atomic velocity. In an alternative "Heisenberg Microscope" configuration an incident thermal beam produces a velocity average over different fringe Fourier components. AC modulated weak laser light passing through the interferometer interacts selectively with atoms at a specific velocity. The associated fringe pattern is then AC modulated and revealed by its selective destruction.

1. INTRODUCTION

Fundamental to the foundations of quantum mechanics is the notion that particles propagate as matter waves (deBroglie waves). Indeed, Davidson and Germer's surprising discovery that electrons are diffracted by crystals forced the development of the mathematical framework for quantum theory, which has since become a cornerstone of modern physics. Interferometers for electrons[1] and neutrons[2] are now commonplace in many physics laboratories. Although initially a neutron was thought to be an elementary particle, it is now believed that a neutron is a "composite" particle that is a bound state of quarks. One may ask whether even more complicated composite particles such as atoms and molecules demonstrate matter-wave interference in a manner similar to that of a neutron, electron or photon, even when the "size" of such a particle is bigger than its deBroglie wavelength. Indeed, an atom such as potassium is a very complicated thing. It contains electrons, virtual photons, nucleons, mesons, quarks, gluons, and lots of virtual stuff, some of which we may have not even yet identified. How do big composite particles such as whole atoms exhibit spatial deBroglie-wave interference? The Hamiltonian for such a beast is a sum over the kinetic and internal potential energies of the atom's

0-8194-1673-8/94/$6.00

constituent parts. By the *magic* of the center-of-mass transformation in quantum mechanics, this sum can be split into a sum of two parts[3]. The first part is the Hamiltonian studied by spectroscopists, while atom interferometry experiments exploit the second part (or both parts). This second part represents the kinetic energy of a moving point-particle, whose mass, m, is that of the whole atom. Then, via deBroglie's relation, atom matter waves propagate with a deBroglie wavelength given by $\lambda_{dB} = h / (m v)$, where h is Planck's constant and v is the atom's velocity. Experiment now shows that despite an atom's extremely complicated structure, it demonstrates deBroglie wave interference, and simultaneously remains a whole atom, even after it passes simultaneously through more than one slit.

Interference of atom matter waves was first observed by Estermann and Stern[4] in the diffraction of atoms by the face of a crystal. With well collimated atomic beams Leavitt and Bills[5] observed Fresnel diffraction of by an edge. Similarly, Gould *et al.*[6] observed Fraunhofer diffraction by a standing-wave laser acting as grating (via the Kapitza-Dirac effect), and Kieth *et al.*[7] observed Fraunhofer diffraction by a microfabricated solid grating. Early proposals to build deBroglie-wave atom interferometers were given by Altshuler and Frantz[8], Dubetskii *et al.*[9], and Clauser[10]. Recently, Carnal and Mlynek[11] and Shimizu *et al.*[12] built atom deBroglie wave analogs of Young's classic optical experiment and produced interference fringes upon transmitting the atoms through two separated slits. Kieth *et al.*[13] used transmission gratings to split a fast atomic beam into two beams, to reconverge the beams to form fringes, and finally to mask the fringes to allow their detection. By applying laser radiation pulses at various times during the propagation of an atomic beam, Kasevich and Chu[14] separated and recombined atomic propagation paths to produce spatial interference. By applying laser radiation at various spatial positions along a beam, Sterr *et al.*[15] and Riehle *et al.*[16] demonstrated similar interference effects.

2. INTERFEROMETRY USING A COLD SLOW ATOM SOURCE

In this paper we present the results of two different experiments demonstrating atom matter-wave interference[17]. Our interferometer employs a recent generalization by Clauser and Reinsch[18] of the Talbot and vonLau effects. That work is summarized here in an Appendix. Our apparatus for the first experiment is diagramed in Fig. 1. Two copropagating potassium beams pass simultaneously through an atom interferometer and are detected by surface ionization on a hotwire[19]. The first is temporally continuous (DC), and has a thermal velocity distribution broadly peaked at about 540 m/sec. It acts as a "parent" for the second beam. The second beam is temporally chopped (AC) and synchronously detected to allow it to be distinguished from the first. The AC beam is slow ($v \approx 182$ m/sec) and cold. The DC thermal beam is produced by an oven. The oven's exit slit is offset from the interferometer axis, with the transmitted DC flux produced by scattering near that slit. Nonetheless, the transmitted thermal beam current is still about 130 times stronger than that of the slow beam. The latter is velocity selected by using AC modulated (chopped ON and

OFF at 6 Hz) laser light, incident on the thermal beam at 20°. Scattering of about 7 photons by each slow atom deflects it out of the low velocity portion of the parent beam's thermal distribution, onto the interferometer's axis. The parallel component of the laser's incidence provides Doppler velocity selection, while the perpendicular component provides momentum transfer for deflection. The effective source brightness for cold 182 m/sec atoms is about 4×10^{15} atoms cm^{-2} sr^{-1} sec^{-1}, yielding a maximum transmitted and detected current of roughly 4×10^{5} atoms per sec.

The interferometer consists of a sequence of three parallel planes, each containing a rectangular vacuum-slit transmission grating, G_1, G_2, and G_3, respectively. The spacings between the grating planes are $R_1 = R_2 = 46.2$cm. The gratings are micro-fabricated from 1μ thick silicon-nitride membranes supported by silicon frames, with parallel slits (of width δ) etched through the membranes. Gratings G_1 and G_3 have the same period, $a_1 = a_3 = 16.2\mu$, and have 22 and 76 slits, respectively. Grating G_2 has 111 slits, with a period, $a_2 = 8.1\mu$. All three are 8.5 mm long and have an average open fraction of about $\delta/a = 1/8$.

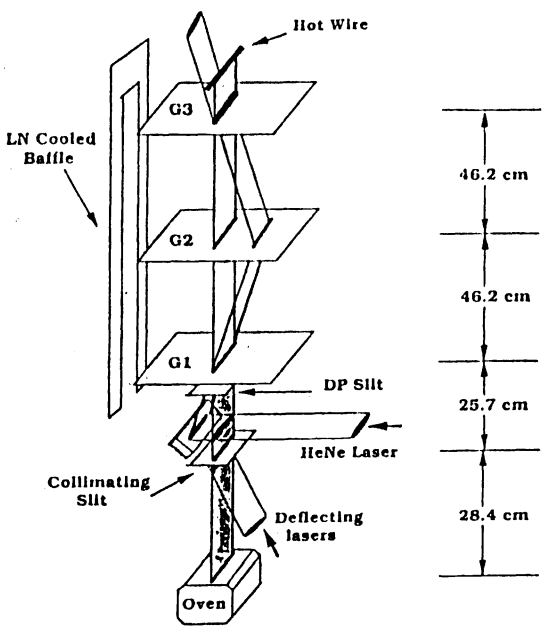

Fig. 1. Geometry of the experimental apparatus used for experiments with a cold slow incident atomic beam. A HeNe laser beam passing through the gratings is used for rotational alignment of the interferometer.

For an interferometer with the above geometry Reinsch and Clauser[20] pointed out that deBroglie-wave fringes will be formed on and masked by G_3 via the generalized Talbot-vonLau effect (See Appendix). Fringes are sensed by monitoring the variation of the transmission in response to slowly scanning G_2's position. An interfering path set within the beam envelope consists of nested diamonds, starting at one source slit of G_1 and forming an interference pattern on G_3.

Solid-angle acceptance is enhanced (by a factor of almost 10^7 over the atom interferometer geometry used by Ref. 13) by incoherent addition of the current from many source slits on G_1, each providing many such nested diamonds at all possible skew angles between the slits of G_1 and G_2.

In the high velocity limit ($n \to 0$), the geometric shadows superpose and form a simple Moiré. As indicated above, with low velocity monochromatic illumination an interference pattern is also formed. The fringe pattern (and the transmitted current) contains various spatial harmonics of the geometric shadow Moiré period. Each harmonic will be resonant in the interferometer at a different atomic velocity. Figure 2a shows possible velocity profiles for the AC beam produced by our source, while Figure 2b shows the calculated amplitudes for the 4th, 5th and 6th harmonic components of a Fourier decomposition of the pattern as a function of atomic velocity. A resonance for the m'th harmonic occurs at $\lambda_{dB}/\lambda_{TR} = n/m$ when m and n approximate small integers. Here, λ_{dB} is the atoms' deBroglie wavelength, $\lambda_{TR} \equiv a_2^2/\rho$ is the interferometer's Talbot-Rayleigh wavelength, and $\rho \equiv R_1R_2/(R_1+R_2)$ is the interferometer's reduced length. For our geometry the associated resonant atomic velocity is $m/n \times v_{TR}$, where $v_{TR} \approx 35$ m/sec. Phase reversal of the (m,n) = (5,1) resonance (5'th harmonic) is a consequence of the fact that the product, $m \times n$, is odd.

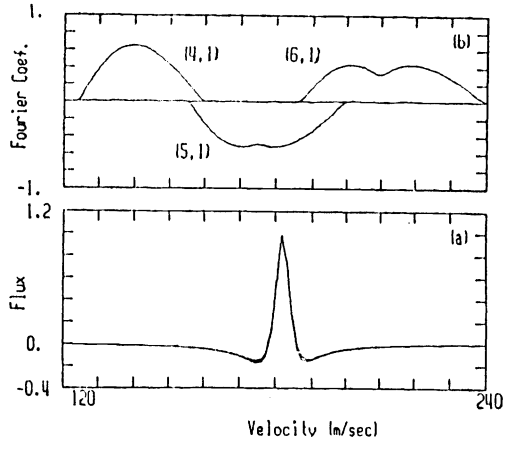

Fig 2b. 4th, 5th, and 6th spatial harmonic content of the calculated fringe pattern at the respective (m,n) = (4,1), (5,1) and (6,1) interferometer resonances.

Fig. 2a. Two possible velocity profiles for our source, assuming a parallel velocity spread of about 10 - 12 m/sec. Positive and negative signs correspond to in-phase and phase-reversed AC signal levels.

Figure 3 shows for various atomic velocities the calculated interferometer transmission as a function of G_2 displacement, averaged over the finite slit widths G_1 and G_3. At velocities above $a_2/\Delta_2 \times v_{TR} \approx 8\ v_{TR} \approx 278$ m/sec, the oscillatory fringe structures give way to the ($n \to 0$) geometric shadow. The calculated AC and DC signals at any grating position are given by a weighted integration of the transmission over atomic velocity. For the AC signal, a weighting

by the velocity profile of Fig. 2a samples a narrow range of the velocities where high frequency oscillatory fringe structures occur. A thermally distributed weighting yields a diffraction limited geometric Moiré for the DC fringe pattern.

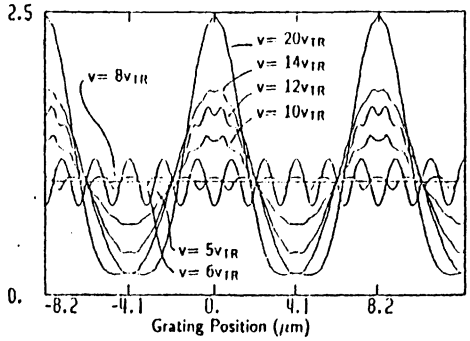

Fig. 3. Calculated normalized interferometer transmission as a function of and grating displacement, for various atomic velocities, 175, 210, 280, 350, 419, 489, and 699 m/sec, corresponding to 5, 6, 8, 10, 12, 14, and 20 times v_{TR}, respectively.

Figure 4a shows the measured (solid) and calculated (dashed) DC signal as a function of grating position, while Fig. 4b shows the simultaneously measured AC signal in response to a single scan of G_2's position. Each data point represents about a 4 sec integration. Due to a start-up hysteresis in our piezoelectric translator, the G_2 displacement axis suffers from a nonlinear distortion for negative values, evident in both the AC and DC signals. Despite this distortion a fifth spatial-harmonic component is evident in the AC signal. Since the laser tuning selects atoms near the (m,n) = (5,1) resonance, this harmonic is expected to dominate. However, given the v^3 weighting of atoms in the parent beam, the phase-reversed high-velocity broad Lorentzian wing of the profile contributes significant sixth harmonic at opposite phase that enhances end fringes and washes out central fringes. Figure 5b also shows the associated calculated AC fringe patterns for the two assumed incident AC velocity profiles of Fig. 2a.

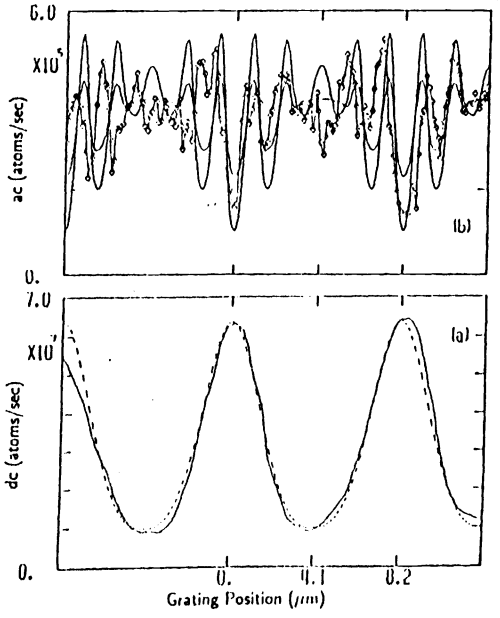

Fig. 4b. Measured AC signal (diamond points) and calculated AC signals (with the vertical offsets suppressed), for the different assumed velocity distributions of Fig. 2a.

Fig. 4a. Simultaneously measured (solid line) and calculated (dashed line) DC signal as a function of grating relative displacement. Zero level corresponds to the laser-blocked condition.

Since the interferometer is highly velocity selective, a small change in the excitation spectrum has a strong effect on the shape of the AC fringe pattern, and a wide variety of patterns composed of various spatial harmonics may be produced by selecting different atomic velocities with the deflecting laser(s). The asymmetry and finite visibility of the DC fringe pattern are due dominantly to quantum-mechanical diffraction by G_2 and more weakly to geometrical averaging by G_1 and G_3.

3. "HEISENBERG MICROSCOPE" DECOHERENCE ATOM INTERFEROMETRY

Recently, Walls *et al.*[21] analyzed a problem, analogous to that of the "Heisenberg microscope", for freely propagating atoms with well defined momenta that form deBroglie-wave fringes in a Young's two-slit interferometer. They consider a situation wherein both slits are simultaneously illuminated with light that is resonant with an atomic transition, and calculate the resulting atomic fringe visibility as a function of slit separation. They predict that when the slits are separated sufficiently, so that a Heisenberg microscope viewing the reemitted fluorescence can image this light to determine which slit an atom passes, then the atomic fringe visibility will vanish. But when the slit spacing is comparable to the optical wavelength, such a determination by the microscope exceeds its resolving power, and then the interference pattern will persist. Further, the presence of the microscope is unnecessary for the predicted visibility dependence on slit spacing to obtain (none is present in our experiment). Only the microscope's illumination need be present.

The above predictions can be tested. Indeed, Sterr *et al.*[15] destroyed atom interference fringes by passing high intensity resonant laser light through their atom interferometer. In that experiment many photons were scattered off of each atom, and while their atomic paths have an amplitude for being physically separated in space, actually the paths are continuously distributed in space and are not clearly localized by a scattering event. In our experiment we destroy atom interference fringes by the scattering of a single low energy photon by an atom. In our experiment with no microscope illumination (and no scattering), amplitudes for an atom's passage simultaneously through more than one physically different slit provide quantum interference and produce a multiple slit interference pattern. With illumination, however, a scattering can localize an atom's path to a region smaller than our slit spacing. Within our multiply connected geometry an atom, thus localized, can pass through only one slit. Hence the scattering can be used to determine which slit the atom passes, whereupon no fringe pattern will form.

The above process is used by our second atom interferometry experiment. A high spatial frequency interference fringe pattern is revealed by its destruction. In this experiment only a thermal potassium beam is transmitted through the atom interferometer used

above. Atoms at characteristic resonant atomic velocities and/or deBroglie wavelengths form fringe patterns that contain high spatial-frequency Fourier components. However, the thermal velocity distribution produces an average over these components that washes-out and hides the high frequency fringes. AC modulated laser light now passes through the interferometer near G_2. Since imaging of the fluorescent light could be used to determine which G_2 slit an atom passes, the contribution to the averaged pattern by atoms at the laser's Doppler shifted wavelength is removed. That component is thus AC modulated and detected. Potassium's hyperfine structure effectively limits the number of scatterings per atom to about one via the high probability that following a scattering the atom will optically pump and thereafter be transparent to the laser radiation[22]. To further assure only one scattering per atom in an atom's flight time through the laser beam, and to provide a narrow effective laser bandwidth, the laser is attenuated heavily.

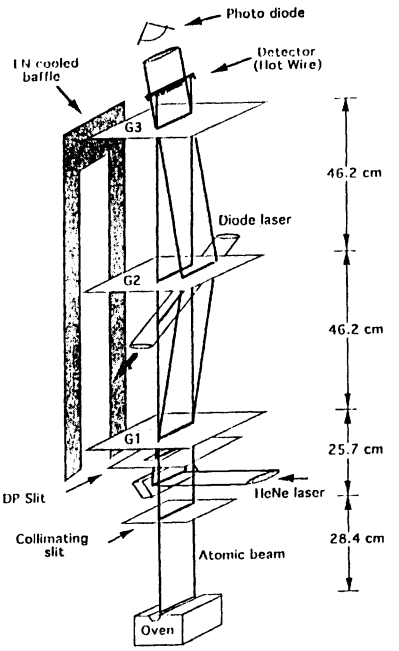

Fig. 5. Geometry of the experimental apparatus for the Heisenberg microscope experiments. Photomultiplier used to measure fluorescence intensity is not shown.

The apparatus, shown in Fig 5., is a modification of that of Fig. 1. The oven is now located on the axis and the deflecting laser light is not used. Instead, "microscope illumination" consists of a highly attenuated AC chopped laser beam passing through the interferometer at near anti-parallel incidence (20°) to the beam, immediately below G_2. When the laser is (OFF), then interference fringes are formed, but the beam's thermal velocity average prevents their direct observation. When the laser is ON, it resonates with two different velocity groupings of atoms, since K^{39} has two atomic ground-state hyperfine levels (F=1,2). F = 2 atoms will be resonant only for tunings with v greater than 351m/sec, the velocity Doppler equivalent of the hyperfine resonance spacing.

We calculate the laser-ON transmission probability, assuming a kinematical scattering near G_2 of one photon by each atom, assume a classical atomic trajectory, and use the point-wise momentum-transfer photon scattering model by Einstein[23] in his discussion of the kinematics required for thermal equilibrium to obtain when a gas is irradiated by thermal light. The transmitted AC current, is given by the difference between this transmission probability and that for no laser light, averaged over the thermal velocity distribution, and weighted by the probability that an atom will scatter one (and only one) photon in an atom's transit through the laser beam. This probability has two resonant near-Lorentzian components separated by 351 m/sec, corresponding to and weighted by the thermal hyperfine level populations, 40% F = 1 and 60% F = 2.

To observe interference fringes, the laser is tuned to resonate with F = 1 atoms at a velocity of 211 m/sec, i.e. 6 times the Talbot-Rayleigh velocity, $v_{TR} \approx 35$ m/sec, corresponding to AC fringes at the sixth spatial harmonic of the geometric shadow period. While holding the laser tuning constant, G_2 is scanned laterally, and the DC and AC signals are recorded simultaneously. These signals are shown as a function of G_2 displacement, Δx, in Figs. 6a and 6b, along with the calculated DC and AC currents. The sixth spatial harmonic associated with the Talbot-vonLau resonance is evident in the AC signal's data.

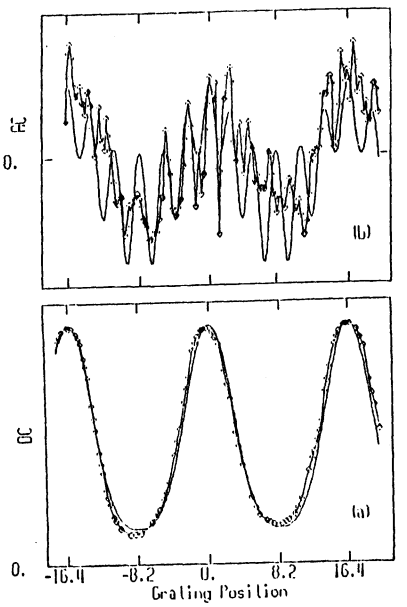

Fig. 6b. Calculated and observed (diamond points) AC atomic current as a function of grating relative displacement, Δx (microns), showing the destroyed fringes for atoms at 211 m/sec. To give better agreement between the observed and calculated AC patterns, a small DC signal cross-talk component is added to the calculated AC signal.

Fig. 6a. DC signal due to thermal beam illumination.

To observe the velocity dependence of the AC signal, G_2's position is held fixed and the laser tuning is swept. The measured signals obtained when the gratings are positioned for minimum and maximum transmitted DC current are shown in Figs. 7a and 7b, along

with the calculated signals. Agreement between the calculated and measured signals appears to be quite good.

For comparison, in Fig. 7c we show the laser excited fluorescence intensity measured using a photomultiplier and the same laser incidence angle (but with no gratings present) in response to a similar laser frequency scan. We note that the hyperfine structure is not resolved in the fluorescence spectrum. By contrast, the transmission spectrum of Fig. 7a. displays two well-resolved peaks whose the spacing corresponds to the hyperfine structure. Evidently we have constructed what amounts to an atom interference filter, whose velocity selectivity allows us to narrow the effective transmitted velocity range, so as to provide an improvement in the atom-optical spectral resolution. When the gratings are positioned for minimum DC transmission, then neither the laser-ON nor laser-OFF conditions transmit atoms at high velocity. However, the reasons for these high-velocity cut-offs differ. In the laser-ON condition only low velocity atoms have sufficient scattering angle to reach a G_3 open slit. A cut-off via this process then occurs at an atomic velocity of about 740 m/sec. In the laser-OFF condition only atoms with velocities below $\Delta_2/a_2 \times v_{TR} = 278$ m/sec have sufficiently long deBroglie wavelength so that two adjacent G_2 slits produce overlapping constructive interference at an open G_3 slit. The different cut-off velocities (and profiles) effectively create a "pass-band" that allows resolution of the K^{39} hyperfine structure.

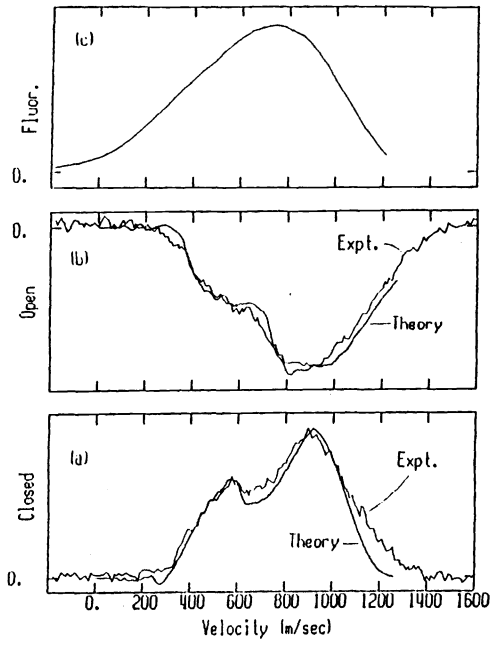

Fig. 7c. Fluorescence intensity as a function laser tuning.

Fig. 7b. Calculated and observed atomic current as a function laser tuning, for fixed grating at maximum DC current.

Fig. 7a. Same as (b) but at minimum DC current.

4. ACKNOWLEDGEMENTS

This work was supported by ONR Grant N00014-90-J-1475 and the Firm J.F. Clauser & Assoc., Walnut Creek, CA. We also acknowledge assistance in this work by M. W. Reinsch, G. Garfein, and the staff and students at the UC Berkeley Microstructures Lab.

5. APPENDIX: GENERALIZED TALBOT - VONLAU EFFECT

In this Appendix, we summarize the recent generalization by Clauser and Reinsch[18] of the theory of the Talbot and vonLau effects. Clauser and Reinsch first considered the simple 2D geometry (in the Fresnel domain) of a monochromatic (with wavelength λ) point source of waves illuminating a periodic (with period a) transmitting planar structure (with a finite number of periods, N), and calculated the amplitude produced at a plane following this structure. The spacing between the source and the diffracting structure is R_1, and between the structure and the "image" plane is R_2. They found the following results:

(1) In any given diffraction geometry, there are four distinct regimes. Proceeding from long to short wavelengths one encounters the Fraunhofer, Fresnel, Talbot-vonLau, and geometric shadow regimes.

(2) In the Talbot-vonLau regime, a fringe "resonance" (of width ε) occurs for $\lambda / \lambda_{TR} = n/m \pm \varepsilon$, when m and n are small integers. At a resonance, each period of the periodic "image" consists of a nearly exact (for modestly large N) magnified self-image of a grating period. Here, $\lambda_{TR} \equiv a^2/\rho$ is the interferometer's Talbot-Rayleigh wavelength, and $\rho \equiv R_1 R_2/(R_1+R_2)$.

(3) Nearly exact self images are formed only when the integer, n, is a divisor of the number of slits, N. Hence it is possible to determine from the diffraction pattern whether the structure contains a prime number of periods.

(4) For a finite number of slits, there is a spatial frequency shift (in the image) relative to that for $N = \infty$.

(5) For values of the integer m not equal to one, the "image" contains m-fold "alias's" of the magnified self-image added per geometric shadow period.

(6) For each period consisting of a simple slit of width, Δ, the resonance width is given by $|\varepsilon| \leq m \Delta n^{-2} a^{-1}$. The resonance boundaries are sharp!

(7) Geometric shadows are formed in the $n \to 0$ limit. The $n = 0$ resonance is also sharp. Its limit occurs at $\lambda / \lambda_{TR} = \Delta / a$.

(8) There is a 180° phase shift (relative to the geometric shadows) whenever the product, m × n, is odd.

(9) A high throughput interferometer can be formed by using a sequence of three gratings, tuned to a Talbot-vonLau resonance and configured so that the fringe pattern produced at the third grating's plane by any slit in the first grating coincides with that produced by any other slit in the first grating.

6. FOOTNOTES AND REFERENCES

[1]L. Marton *et al.* Phys. Rev. **90**, 490 (1953), Rev. Sci. Instr. **25**, 1099 (1954); J. A. Simpson, Rev. Mod. Phys. **28**, 254 (1956); D. Gabor, Rev. Mod. Phys. **28**, 269 (1954).

[2]S. A. Werner, Physics Today **33**, 24 (1980); A. G. Klein and S. A. Werner, Rep. Prog. Phys. **46**, 259 (1983); D. M. Greenberger and A. W. Overhauser, Rev. Mod. Phys. **51**, 43 (1979).

[3]See, for example, A. Messiah, *Quantum Mechanics*, (J. Wiley, New York, 1962), Vol. II, p395, 412.

[4]L. Estermann and O. Stern, Zeits. f. Physik, **61** 95 (1930).

[5]J. A. Leavitt and F. A. Bills, Am. J. Phys., **37**, 905 (1969).

[6]P. L. Gould *et al.*, Phys. Rev. Lett. **56**, 827 (1986).

[7]D. W. Kieth *et al.*, Phys. Rev. Lett. **61**, 1580 (1988).

[8]S. Altshuler and L. M. Frantz, US Patent # 3,761,721.

[9]B. Ya. Dubetskii *et al.*, Pis'ma, Zh. Eksp. Teor. Fiz. **39** (11), 531, (1984).

[10]J.F. Clauser, Physica **B 151**, 262 (1988); US Patents # 4,874,942 and # 4,992,656.

[11]O. Carnal and J. Mlynek, Phys. Rev. Lett. **66**, 2689 (1991).

[12]F. Shimizu *et al.*, Phys. Rev. **A46**, R17 (1992).

[13]D. W. Keith *et al.*, Phys. Rev. Lett. **66**, 2693 (1991).

[14]M. Kasevich and S. Chu, Phys. Rev. Lett. **67**, 181 (1991).

[15]U. Sterr *et al.*, Appl. Phys. Lett. **B54**, 341 (1992).

[16]F. Riehle *et al.*, Phys. Rev. Lett. **67**, 177 (1991).

[17]J. F. Clauser and S. Li. Phys. Rev. A **49**, R2213 (1994); J. F. Clauser and S. Li., to be published.

[18]J. F. Clauser and M. W. Reinsch, Appl. Phys. **B 54**, 380 (1992), and, references therein.

[19]S. Li and J. F. Clauser, Phys. Rev. A **49**, 2702 (1994).

[20]M. W. Reinsch and J. F. Clauser, Bul. Amer. Phys. Soc. **36**, 1312 (1991). See also Ref. 18.

[21]D. Walls, *et al.*, in *Foundations of Quantum Mechanics*, eds. T. D. Black *et al*, (World Scientific, Singapore, 1992), p.157.

[22]Optical pumping is avoided in the first experiment by using a cycling transition, and by applying two laser frequencies for the deflecting light.

[23]A. Einstein, Phys. Zts. **18**, 121 (1917), in B. L. van der Waerden, *Sources of Quantum Mechanics*, (Dover, New York, 1968) p. 63.